Calculation of Fuel Spray Impingement and Fuel Film Formation in an HSDI Diesel Engine

Manshik Kim, Kyoungdoug Min*

School of Mechanical and Aerospace Engineering, Seoul National University, Seoul 151-742, Korea

Spray impingement and fuel film formation models with cavitation have been developed and incorporated into the computational fluid dynamics code, STAR-CD. The spray/wall interaction process was modeled by considering the effects of surface temperature conditions and fuel film formation. The behavior of fuel droplets after impingement was divided into rebound, spread and splash using the Weber number and parameter $K(\sqrt{We}\sqrt{Re})$. The spray impingement model accounts for mass conservation, energy conservation, and heat transfer to the impinging droplets. The fuel film formation model was developed by integrating the continuity, momentum, and energy equations along the direction of fuel film thickness. Zero dimensional cavitation model was adopted in order to consider the cavitation phenomena and to give reasonable initial conditions for spray injection. Numerical simulations of spray tip penetration, spray impingement patterns, and the mass of film-state fuel matched well with the experimental data. The spray impingement and fuel film formation models have been applied to study spray/wall impingement in high-speed direct injection diesel engines.

Key Words: Spray Impingement, Fuel Film Formation, Cavitation, HSDI Diesel Engine

Nomenclature

BTDC : Before top dead center
C : Fuel concentration (kg/kg)
d : Diameter (m)
g : Gravitational acceleration (m/s^2)
h_d : Mass transfer coefficient (kg/m^2·s)
K : Non-dimensional parameter for criterion of splash
La : Laplace number
p : Pressure (Pa)
T : Temperature (K)
U,u,v : Velocity (m/s)
$\bar{u}$, $\bar{v}$: Mean velocity (m/s)
We : Weber number
δ : Fuel film thickness (m)
μ : Dynamic viscosity (kg/m·s)
ν : Kinematic viscosity (m^2/s)
θ : Angle (degree)
ρ : Density (kg/m^3)
σ : Surface tension (N/m)
τ : Shear stress (N/m^2)
ξ : Profile factor

Subscripts

crit : Critical
d : Drop
eff : Effective
f : Film
i : Incoming
l : Liquid
n : Normal
o : Outgoing
s : Splash
t : Tangential
vena : Vena contracta
w : Wall

* Corresponding Author,
E-mail : kdmin@snu.ac.kr
TEL : +82-2-880-1661; **FAX** : +82-2-883-0179
School of Mechanical and Aerospace Engineering, Seoul National University, Seoul 151-742, Korea.
(Manuscript **Received** June 11, 2001; **Revised** December 10, 2001)

1. Introduction

The impingement of fuel spray on the cylinder wall or the piston wall in high-speed direct injection (HSDI) diesel engines is unavoidable. The characteristics of impinging spray are important because they influence fuel vapor distribution, combustion process and exhaust emissions. Wall impingement can cause high hydrocarbon emissions and soot formation in small HSDI diesel engines (Matsui, 1986). Werlberger and Cartellieri (1987) observed the impinging spray in a small bore direct injection diesel engine. They determined that, at high load conditions, more than 50% of the fuel impinged on the piston bowl. Therefore, it is important to fully understand the behavior of an impinging droplet near the wall.

A diesel spray structure consists of three regions. In the atomization zone, the injected fuel is atomized, and dense fuel vapor is generated. The full modeling of atomization process is difficult and requires high computer performance because of its complexity. Over the last few years, numerous studies have revealed that nozzle flow has a decisive impact on the subsequent fuel spray development and atomization. The demand for well atomized fuel spray has led to the development of common rail injection system. However, nozzle hole cavitation seems to be a common feature. Cavitation phenomenon is more prominent at higher injection pressures and smaller nozzle hole sizes. Thus, it is necessary to consider the cavitation effect on the spray injection. Below the atomization region, the characteristics of spray are governed by droplet-droplet and droplet-gas interactions. In the near wall region, rebounding, spreading or splashing of droplets may occur according to impinging droplet conditions.

Furthermore, the deposition of injected fuel spray resulting from spray impingement on the wall causes the fuel film flow. Several phenomenological models for the spray impingement were developed. A better understanding of the spray-wall interaction and the after-impingement behavior of droplets will help improve injection systems and combustion chambers. The objective of this paper is to develop physically reasonable model for spray-wall impingement and fuel film formation. The after-impingement behavior of droplets is determined from experimental results (Mundo *et al.*, 1994, 1995, Yarin *et al.*, 1995).

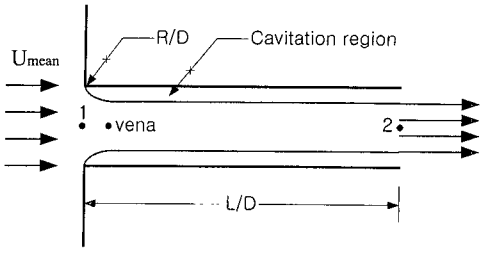

Fig. 1 Schematic diagram of nozzle flow phenomena

In this paper, a model was formulated and validated to describe spray impingement and fuel film formation, which includes cavitation. Experimental data were used to validate the model in more realistic configurations. At the end of the paper, HSDI diesel engine calculations using the fuel film formation model during the compression process for cold start and warm operating conditions are described.

2. Modeling

2.1 Spray injection in consideration of cavitation

Sarre *et al.* (2000) proposed the nozzle flow model, which determines the spray initial conditions such as the discharge coefficient, injection velocity, and initial droplet diameter by incorporating nozzle inlet configuration, cavitation effect, injection flow rate and chamber conditions. In HSDI diesel engines equipped with a common rail injection system, cavitation regime model should be applied. Figure 1 shows a schematic diagram of nozzle flow phenomena. The effective velocity of droplets at the nozzle exit, U_{eff}, and the diameter of initial droplet, d_{eff}, are determined by the following relation.

$$U_{eff} = U_{vena} - \frac{p_2 - p_{vapor}}{\rho_l U_{mean}} \quad (1)$$

$$d_{eff}=d\sqrt{\frac{U_{mean}}{U_{eff}}} \tag{2}$$

U_{vena} is the velocity in the vena-contracta and is determined as follows.

$$U_{vena}=\frac{U_{mean}}{C_c} \tag{3}$$

where C_c is the contraction coefficient, a geometry dependent parameter which has been calculated to be about 0.62, for sharp-edged orifices given by Nurick (1976).

The pressure in the vena-contracta is determined as follows.

$$p_{vena}=p_l-\frac{\rho_l}{2}U_{vena}^2 \tag{4}$$

The pressure in the vena-contracta was below the vapor pressure of the fuel; therefore, the initial conditions were assigned for spray calculation from Eqs. (1) and (2).

The breakup model proposed by Reitz and Diwakar (1986) was used to simulate the droplet breakup processes. O'Rourke's (1981) model was used for the collision and coalescence among droplets.

2.2 Spray/wall interaction model

After a droplet impinges on a surface, the following events occur.

1. The impinging droplet may rebound, changing direction and velocity.
2. For certain impact energy conditions, the droplet deposits on the wall.
3. For higher impact energy conditions, the impinging droplets may splash and form a liquid fuel film, making smaller secondary droplets.

These impingement regimes are characterized by a number of parameters. A set of non-dimensional numbers describes droplet impingement phenomena.

$$We=\frac{\rho d u^2}{\sigma} \tag{5}$$

$$La=\frac{\rho\sigma d}{\mu^2} \tag{6}$$

$$K=We^{0.5}Re^{0.25}=\left(\frac{\rho^3 d^3 u^5}{\mu^2\sigma}\right)^{0.25} \tag{7}$$

where ρ, μ, and σ are the density, the dynamic viscosity, and the surface tension of fuel, respectively. u and d are the velocity and the diameter of a droplet. In this study, the spray impingement model is divided into the hot wall model and the cold wall model to represent low load and high load engine operating conditions. As the impact energy of the impinging droplet increases, the behavior of droplets after impingement was divided into rebound, spread, and splash models. The non-dimensional impact parameters We and K determine the mode type. The diameter and the number of secondary droplets for the splash model are determined based from experimental data.

2.2.1 Cold wall model

When the wall temperature is below the saturation temperature of impinging droplets, the cold wall model is applied.

Splash modeling

The transition criterion for the splashing regime is based on Mundo *et al.*'s experimental results (Yarin *et al.*, 1995).

$$K>57.7 \tag{8}$$

Given incident conditions, we need to determine the total mass, sizes, velocities and ejection angles of secondary droplets. It is assumed that an impinging droplet breaks into four droplets of identical mass but different diameters.

The sizes of the splashing droplets are determined by the probability density function based on experimental data (Mundo *et al.*, 1994).

The total ejected mass of splashing droplets is determined from experimental results (Yarin and Weiss, 1995). Yarin and Weiss showed that the mass fraction of secondary droplets to the impinging droplet is related to a non-dimensional impact velocity. The non-dimensional impact velocity is defined as:

$$\bar{u}=u_n\left(\frac{\rho}{\sigma}\right)^{1/4}\nu^{-1/8}f^{-3/8} \tag{9}$$

where u_n is the droplet normal velocity component and f is the drop frequency.

The mass ratio is given by curve fitting to the data equation (Stanton *et al.*, 1996).

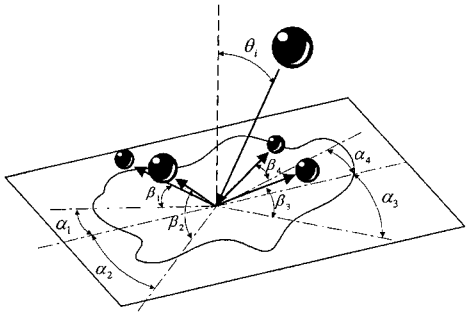

Fig. 2 Schematic diagram of splashed droplet

$$\frac{m_s}{m_d}=-27.2+3.15\bar{u}-0.116\bar{u}^2+0.0014\bar{u}^3 \quad (10)$$

m_s is the mass of splashed droplets and m_d is the mass of the incident droplet.

Mundo *et al.* (1994) investigated the correlation between the incident angle θ_i and the splashing angle θ_o for rough walls. The splashing angle θ_o is given by Eq. (11). Considering the deviation of experimental data, the splashing angle is given at random within $\theta_o \pm 10$ deg.

$$\theta_o=60.0^\circ+0.25\theta_i \quad (11)$$

Figure 2 shows schematic diagram of a splashing droplet. The in-plane angles, α_1, α_2, α_3, and α_4 are randomly chosen to vary between 0 and 30 degrees from the incoming direction. The ejection angles, β_1, β_2, β_3, and β_4 are determined by using Eq. (11).

The splashing droplet velocities are obtained from overall energy conservation:

$$\frac{1}{8}m_s\sum_{i=1}^{4}u_i^2+\pi\sigma\sum_{i=1}^{4}d_iN_i^2=E_{splash} \quad (12)$$

where u_i is the velocity of i-th secondary droplet, N_i is the number of droplets in the i-th parcel. E_{splash} is the splash energy of the incident droplet given by

$$E_{splash}=E_{in}-E_{crit}$$
$$=\frac{\rho}{12}\pi d_o^3u^2+\pi\sigma d_o^2-\frac{\rho}{12}\pi d_o^3u_{crit}^2 \quad (13)$$

where u_{crit} is the critical velocity of incident droplet and is given by Eq. (8).

$$u_{crit}=\left(\frac{57.7\mu^2\sigma}{\rho^3d_o^3}\right)^{0.8} \quad (14)$$

From the data on the size-velocity correlation of splashing droplets provided by Ghadiri (1978), the velocity relation between the splashing droplets is as follows:

$$\frac{u_i}{u_j}=\ln\frac{d_i}{d_o}/\ln\frac{d_j}{d_o}(i,\ j=1\sim4,\ i\neq j) \quad (15)$$

Using Eqs. (12)~(15), the tangential and normal velocities of splashing droplets can be calculated.

Rebound modeling

The transition criterion for the rebounding regime is given by

$$We\leq10 \quad (16)$$

The velocity magnitude and direction of rebounding droplets are determined by using Eqs. (17) and (18).

$$u_t'=\frac{1}{3+6\alpha}u_t^o \quad (17)$$

$$u_n'=-eu_n^o \quad (18)$$

where u_n' and u_t' are the normal and tangential velocities of rebounding droplets, respectively. u_n^o and u_t^o are the normal and tangential velocities of incident droplets, respectively. e is the coefficient of restitution. α is a random number distributed uniformly in the interval (0, 1). The coefficient of restitution is obtained using Eq. (19) as reported by Bai (1995).

$$e=0.993-1.76\theta_i+1.56\theta_i^2-0.49\theta_i^3 \quad (19)$$

where θ_i is the incident angle of droplet measured in radian.

Spread modeling

When the impact energy of an impinging droplet is sufficiently large, the impinging droplet spreads along the wall and forms a fuel film on the wall. This spread regime is given by

$$We>10,\ K\leq57.7 \quad (20)$$

The evaporation rate $\dot{m}$ on the wall is:

$$\dot{m}=h_dA(C_o-C_\infty) \quad (21)$$

where h_d is the mass transfer coefficient and C_o and C_∞ are the concentration of fuel at the interface and at the bulk gas adjacent the fuel film, respectively. The fuel droplet ratio, which remains on the wall, is given by

$$x_r=\begin{cases}1.0(spread)\\ 1.0-m_s/m_d(splash)\end{cases} \quad (22)$$

Mass flux due to the impinging droplets is averaged over the cell area and is used as a source term in the fuel film formation model.

When the following condition is satisfied, spray impingement model regime is changed from the dry wall case to the wetted wall case.

$$\frac{\delta_f}{d_{SMD}}\geq 0.2 \quad (23)$$

The splash, rebound, and spread models, except the splash angle, are basically the same as the dry wall case.

Equation for the splash angle is changed to Eq. (24), based on the experimental data for smooth wall conditions (Mundo *et al.* 1995).

$$\theta_o=61.3^o+0.35\theta_i \quad (24)$$

Considering the deviation of experimental data, the splashing angle is given randomly within $\theta_0\pm$ 10 deg.

2.2.2 Hot wall model

When the wall temperature is above the saturation temperature of an impinging droplet, the hot wall model is applied. When a droplet impinges on a hot surface, the impinging droplet spreads as a fuel film in the radial direction on the wall for a certain period, and thereafter the film shrinks and rebounds or breaks into pieces (Furuya *et al.*, 1998). In the hot wall model, the heat transfer from the wall to one impinging droplet, Q, is given by

$$Q=\alpha_d S_d \tau_d \Delta T \quad (25)$$

where α_d is the average heat transfer coefficient determined according to the superheating value $\Delta T_{sat}(=T_w-T_{sat})$ (Senda *et al.*, 1988). S_d is the averaged contact area, which is obtained from experimental data and τ_d is the residence time of the droplet in film state on the wall (Senda *et al.*, 1994).

With the use of Eulerian-Lagrangian approach, the impinging spray evolution was calculated. The droplet phase was calculated by using the Lagrangian approach, which tracked a sufficiently large number of parcels (2000~5000)

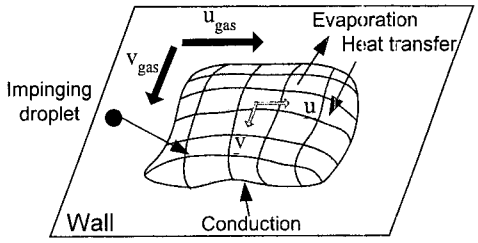

Fig. 3 Physical phenomena governing fuel film flow

(Amsden *et al.*, 1989) representing a number of real droplets having the same diameter and velocity. The equations of motion for the parcels were solved for each time step, using the fluid properties at the current droplet position, as solved for the continuous phase. This led to a new droplet position, for which the procedure was repeated. Seventeen subroutines describing the droplet behavior were incorporated into the STAR-CD code.

2.3 Fuel film formation model

Naber and Farrell (Naber *et al.*, 1993) showed that evaporative wetting phenomena exist at conditions similar to that in internal combustion engines, which is characterized by thin liquid film. Thus, spray impingement models should include liquid films on the combustion chamber surfaces to accurately model spray-wall interactions. The continuity, momentum, and energy equations are applied to each wall cell as shown in Fig. 3. Also, the physical processes affecting the liquid film are shown in Fig. 3.

The numerical solution of the Eqs. (26) ~ (29) can be performed within a two -dimensional framework using thir. film assumption.

$$\frac{\partial u}{\partial x}+\frac{\partial v}{\partial y}+\frac{\partial w}{\partial z}=0 \quad (26)$$

$$\frac{\partial u}{\partial t}+u\frac{\partial u}{\partial x}+v\frac{\partial u}{\partial y}+w\frac{\partial u}{\partial z}=-\frac{1}{\rho}\frac{\partial p}{\partial x}+\nu\frac{\partial^2 u}{\partial z^2}+g_x+a_x \quad (27)$$

$$\frac{\partial v}{\partial t}+u\frac{\partial v}{\partial x}+v\frac{\partial v}{\partial y}+w\frac{\partial v}{\partial z}=-\frac{1}{\rho}\frac{\partial p}{\partial y}+\nu\frac{\partial^2 v}{\partial z^2}+g_y+a_y \quad (28)$$

$$\rho c_p\left(\frac{\partial T}{\partial t}+u\frac{\partial T}{\partial x}+v\frac{\partial T}{\partial y}+w\frac{\partial T}{\partial z}\right)=k\frac{\partial^2 T}{\partial z^2} \quad (29)$$

In deriving the integral conservation /transport Eqs. (26) ~ (29) for a liquid film flow, taking into account the mass, momentum and energy fluxes due to spray impingement and momentum exchange with the gas phase, the following assumptions are applied.

(1) The liquid film is thin enough so that the boundary layer approximations are applicable.

(2) Spray impingement contributes to liquid film transport through deposition of mass, tangential momentum, and thermal energy. These quantities are treated as source terms for each equation.

(3) Liquid surface tension effect on the interfacial momentum is neglected.

(4) The mass flux due to impinging droplets is averaged over the wall cell area. The lost tangential momentum of impinging droplets is added to the film tangential momentum.

By integrating across the film thickness and using thin film assumptions, the equations are reduced to a two-dimensional film flowing across a three-dimensional surface.

After integrating in the cross film direction, Eq. (26) is transformed into the following form:

$$\frac{\partial \delta}{\partial t}+\frac{\partial}{\partial x}(\delta\bar{u})+\frac{\partial}{\partial y}(\delta\bar{v})=source \quad (30)$$

δ is the film thickness and $\bar{u}$, $\bar{v}$ are the averaged film velocities cross the film thickness. The source term is composed of the mass influx of impinging droplets, the mass eflux due to splashing droplets, and fuel vaporization.

Eqs. (27) and (28) are transformed into the following form:

$$\frac{\partial}{\partial t}(\delta\bar{u})+\zeta_p\frac{\partial}{\partial x}(\delta\bar{u}^2)+\zeta_p\frac{\partial}{\partial y}(\delta\bar{u}\bar{v})$$
$$=-\frac{\delta}{\rho}\frac{\partial p}{\partial x}+\frac{1}{\rho}(\tau_\delta(u)-\tau_w(u))+(g_x+a_x)\delta \quad (31)$$
$$\frac{\partial}{\partial t}(\delta\bar{v})+\zeta_p\frac{\partial}{\partial x}(\delta\bar{u}\bar{v})+\zeta_p\frac{\partial}{\partial y}(\delta\bar{u}^2)$$
$$=-\frac{1}{\rho}\frac{\partial p}{\partial y}+\frac{1}{\rho}(\tau_\delta(v)-\tau_w(v))+(g_y+a_y)\delta \quad (32)$$

where ζ_p is the shape factor determined by using a third order velocity profile.

First terms in the right-hand side of Eqs. (31) and (32) represents pressure gradient due to the spray impact on the liquid film interface. If n is denoted as the number of droplets, which have reached the cell adjacent to the wall during the time interval Δt, the impact pressure is given by:

$$p_l=\frac{4\pi\rho_d}{3A\Delta t}\sum^{n} r_i^3 u_n \quad (33)$$

where r_i is the radius of the i-th incident droplet and u_n is its normal velocity. The gas may also induce an impact pressure. This pressure p_g has been derived from impacting liquid jet on a wall as follows (Darrozes *et al.*, 1982).

$$p_g=\rho_g(\vec{u}_g\cdot\vec{n})^2 \quad (34)$$

where ρ_g is the gas density and $\vec{u}_g$ is the gas velocity relative to the fuel film motion.

The energy balance equation at liquid film surface has the follwing form :

$$-kA\frac{\partial T}{\partial z}\Big|_\delta-\dot{m}L=hA(T_\delta-T_\infty) \quad (35)$$

where T_δ is the temperature at the fuel film surface and L is the latent heat of vaporization. T_δ has the following form :

$$T_\delta=\frac{8kA\bar{T}-3kAT_w-\dot{m}L\delta+hAT_\infty\delta}{hA\delta+5kA} \quad (36)$$

where $\bar{T}$ is the is the average film temperature cross the film thickness, T_w is the wall temperature, k is the liquid film thermal conductivity, and A is the wall cell area. Thus, after integrating with respect to cross film coordinate z, the energy equation is

$$\rho c_p\left(\frac{\partial}{\partial t}(\delta\bar{T})+\zeta_T\frac{\partial}{\partial x}(\delta\bar{u}\bar{T})+\zeta_T\frac{\partial}{\partial y}(\delta\bar{v}\bar{T})\right)$$
$$=-\frac{6k}{\delta}[2(\bar{T}-T_w)-(T_\delta-T_w)]$$
$$+m_d\left[\frac{c_p(T_d-\bar{T})}{A\delta dt}\right](1-x_r) \quad (37)$$

where ζ_T is the shape factor determined by using a third order temperature profile. The second term on the right-hand side of the Eq. (37) is the energy source term due to impinging spray. Equations. (30) ~ (32) and (37) are numerically solved by using a fourth order Runge-Kutta scheme.

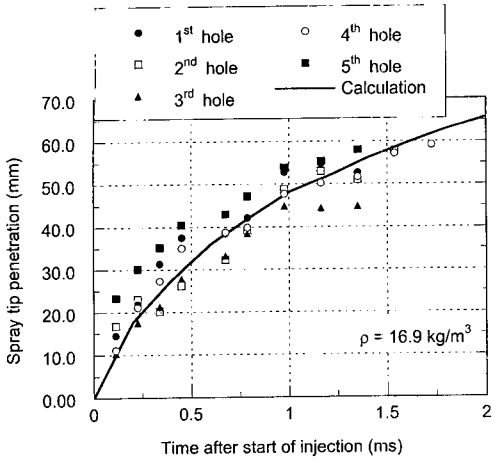

Fig. 4 Comparison of spray tip penetration with experimental data (Bae, 2000)

3. Verification of Models

3.1 Spray tip penetration

A diesel spray injection experiment in a pressurized chamber (Bae, 2000) was adopted to verify the spray initial condition model. In this experiment, the global characteristics of diesel spray emerging from 5-hole VCO nozzle, (e.g. spray angle, tip penetration, and pattern) were measured from the spray images which were frozen by an instantaneous photography with a spark light source. Initial conditions of injected droplets were given by Eqs. (1) and (2). The calculated and measured results of spray tip penetration are shown in Fig. 4. Though the variations of spray tip penetration exist for each hole, the calculation results accurately predict penetration length and spray breakup postion.

3.2 Diesel spray impingement

The present model was also validated against the diesel spray impingement experimental data under elevated pressure and room temperature conditions (Katsura *et al.*, 1989). The investigators applied a laser light extinction method to obtain the photographs of the spray's temporal behavior. Calculation conditions are given in Table 1. Figure 5 shows the experimental and calculated results of diesel spray impingement at 0.8, 1.2 and 2.0 ms after the start of injection.

Table 1 Calculation conditions for diesel impinging sprays

Wall distance (mm)	24.0
Injection duration (ms)	1.2
Injected fuel mass (mg)	7.98
Injection angle (deg)	90
Injected fuel	Diesel fuel
Gas density (kg/m^3)	18.5 air

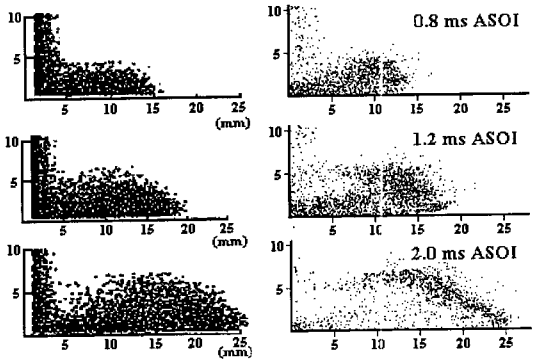

(a) Experiment (b) Calculation

Fig. 5 Comparison of spatial distribution of droplet parcels

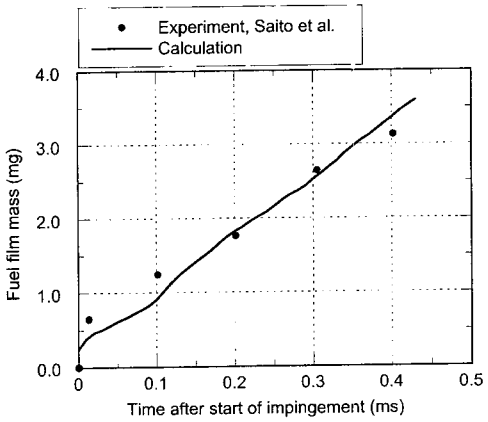

Fig. 6 Comparison of fuel film mass with experimental data (Saito, 1993)

The calculation results predict the spray radius, height and vortex formation at the leading edge.

3.3 Fuel film formation

To verify the film formation model, we used the experimental results of Saito *et al.* (1993). This investigation involved injections in a pressurized chamber under conditions closely approximating

Table 2 Calculation conditions for HSDI diesel engine

Engine speed (rpm)	1500, 4000
Bore (mm)	87.5
Stroke (mm)	87
Compression ratio	19.6
Global equivalence ratio	0.5
Wall temperature (K)	350,500
BDC swirl ratio	2.0, 3.0

those in diesel engines. Figure 6 shows the calculated and experimental variations of wall fuel film mass vs. time. A good agreement is observed for fuel film mass.

4. HSDI Diesel Engine Calculation

Fuel sprays injected into an HSDI diesel engine are also numerically simulated using the spray initial condition model, the spray impingement model, and the fuel film formation model. The model engine used in this study is an HSDI diesel engine having a concentric bowl in the piston. The opening diameter of the bowl is 44 mm and its depth is 13 mm. The fuel is normal-dodecane and is injected into the cylinder in the late period of compression stroke at a constant injection rate. To investigate the effect of injection timing we set the start of injection to 15° BTDC and 3° BTDC. The size and initial velocity of the injected droplets are obtained from Eqs. (1) and (2). The number of injected droplet parcels is 6000. As the initial condition of the gas flow inside the cylinder, the swirl flow is given at the BDC of the compression stroke. The initial cylinder temperature is set at 320 K and the initial cylinder pressure is varied according to the engine speed. The piston wall temperature is set at 500 K and 350 K to calculate warm and cold operations. Calculation conditions and engine specifications are shown in Table 2. The computational mesh of the HSDI diesel engine combustion chamber at 15° BTDC, which consists of 11,232 cells, is illustrated in Fig. 7.

The spray development patterns for different engine speed are shown in Fig. 8. In the 1500 rev/min case, the fuel spray impinges onto the piston

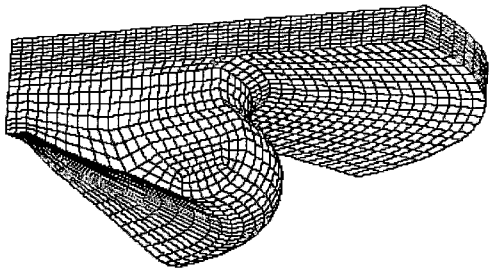

Fig. 7 Computational mesh for HSDI diesel engine calculation

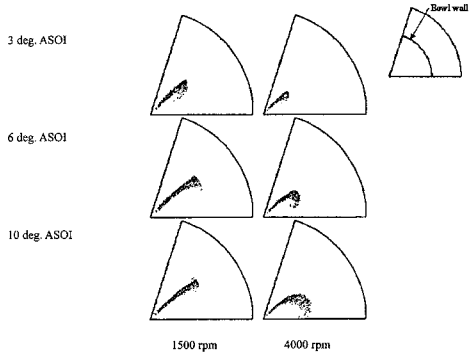

Fig. 8 Spray impingement pattern development for HSDI diesel engine case (a) 1500 rev/min (b) 4000 rev/min (BDC swirl ratio = 3. 0)

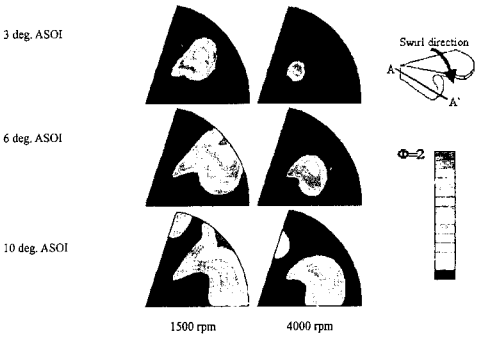

Fig. 9 Fuel vapor distribution for HSDI diesel engine case (a) 1500 rev/min (b) 4000 rev/min

bowl wall and forms a fuel film. In the 4000 rev/min case, the fuel spray does not impinge onto the piston bowl wall. This is due to high tangential velocity in the piston bowl and reduced spray penetration length because of higher cylinder pressure and temperature at the injection period than 1500 rev/min case. In Fig. 9, the fuel vapor concentration is plotted along the plane, which

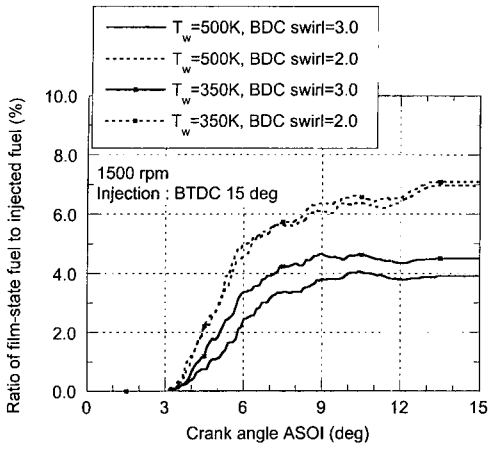

Fig. 10 Calculation of fuel film mass with respect to wall temperature and BDC swirl ratio (Injection timing : 15° BTDC.)

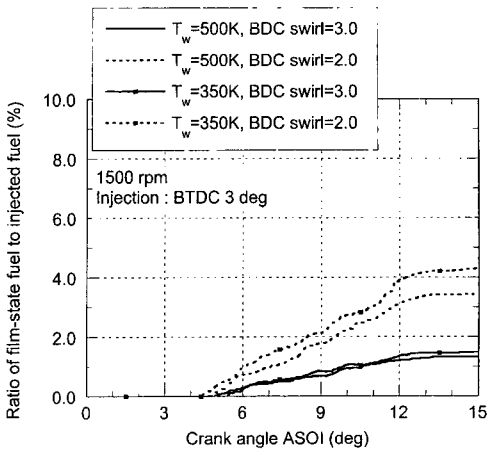

Fig. 11 Calculation of fuel film mass with respect to wall temperature and BDC swirl ratio (Injection timing : 3° BTDC.)

includes the injection axis. The dispersion and spatial distribution of fuel vapor concentration are enhanced not only by swirl motion but also by spray impingement. The vapor cloud and most of the droplets are carried in the direction of swirl rotation. Dense fuel vapor is observed in the near wall region due to evaporation from fuel film and splashed small droplets in the 1500 rev/min case.

Figure 10 shows the ratio of film-state fuel to the injected fuel for the wall temperature and BDC swirl ratio at early injection timing (15° BTDC). A fuel film is formed initially about 3.0 deg after the start of injection. For large swirl ratio and high wall temperature, the mass of fuel film is reduced because many droplets are carried away directly by the gas flow in the near wall region without impinging the wall at all. The BDC swirl ratio is more dominant than the wall temperature in reducing film-state fuel. Figure 11 shows the ratio of film-state fuel to injected fuel for the wall temperature and BDC swirl ratio at late injection timing (3° BTDC). A fuel film is formed initially about 4.5 deg after the start of injection and shows the same trend as Fig. 10. As injection timing is retarded to TDC, the adhered fuel mass (and thus also the average film thickness) is reduced because the spray penetration length is shortened, and evaporation of droplets is enhanced. This spray impingement model with fuel film formation can provide a tool to design combustion chambers and injection strategies.

5. Conclusions

A spray impingement model considering fuel film formation on the wall and cavitation phenomena was developed and validated. The model was validated against experimental data. In all cases, the predictions compared well with the experimental results. It can therefore be concluded that the model presented in this study is useful in predicting spray impingement events and fuel film formation. In addition, HSDI diesel engine simulations were presented in an attempt to demonstrate the capabilities of the spray impingement and fuel film formation models.

(1) A spray impingement model considering fuel film formation on the wall was developed and validated using diesel spray experimental data.

(2) Proposed models were applied to the HSDI diesel engine. The film formation time after the start of injection and the amount of film state fuel was examined. Larger BDC swirl ratio and higher wall temperature reduce the amount of the fuel film on the piston bowl wall.

(3) In 4000 rpm case, spray impingement does not occur because of high tangential velocity in

the piston bowl.

(4) In 1500 rpm case, advanced injection timing increases the amount of the fuel film on the piston bowl.

Acknowledgment

This work was partially supported by the Brain Korea 21 Project, G7 Project and the Institute of Advanced Machinery and Design, Seoul National University, Korea.

References

Amsden, A. A., O'Rourke, P. T., and Butler, T. D., 1989, "KIVA-II : A Computer Program for Chemically Reactive Flows with Spray," Technical Report LA-11560-MS., 1989, Los Alamos National Laboratory Report.

Bae, C. and Kang, J., 2000, "Diesel Spray Development of VCO Nozzles for High Pressure Direct-Injection," SAE Paper No. 2000-01-1254.

Bai, C. and Gosman, A. D., 1995, "Development of Methodology for Spray Impingement Simulation," SAE paper No 950283.

Darrozes, J. S. and Fransois, C., 1982, "Mēcanique des Fluides Incompressibles," Lecture Notes in Physics, Springer-Verlag.

Furuya, M., Kinoshita, I., and Nishi, Y., 1998, "Vapor Explosion in the Droplet Impingement System," Proceedings of 11th IHTC, Vol. 5, pp. 471～476.

Ghadiri, H., 1978, "Raindrop Impact, Soil Splash and Cratering," Ph. D Thesis, University of Reading

Katsura, N. Saito, M., Senda, J., and Fujimoto, H., 1989, "Characteristics of a Diesel Spray Impinging on a Flat wall," SAE Paper No 890264.

Matsui, Y. and Sugihara, K., 1986, "Sources of Hydrocarbon Emissions from a Small Direct Injection Diesel Engines," *JSAE Review*, 1986, Vol. 7, pp. 4～11.

Mundo, C., Sommerfeld, M. and Tropea, C., 1995, "Droplet-Wall Collisions: Experimental Studies of the Deformation and Breakup Process," *Int. J. Multiphase Flow*, Vol. 21, No. 2, pp. 151～173.

Mundo, C., Sommerfeld, M. and Tropea, C., 1994, "Experimental Studies of the Deposition and Splashing of Small Liquid Droplets Impinging on a Flat Surface," ICLASS-94, pp. 134～141.

Naber, J. D. and Farrell, F. V., 1993, "Hydrodynamics of Droplet Impingement on a Heated Surfaces," SAE Paper No 930919.

Nurick, W. H., 1976, "Orifice Cavitation and its Effect on Spray Mixing," *J. of Fluid Engineering*, vol.98, pp. 23～78.

O'Rourke, P. J., 1981, "Collective Drop Effects on Vaporising Liquid Sprays," Ph D Thesis, Princeton University.

Reitz, R. D. and Diwakar, R., 1986, "Effect of Drop Breakup on Fuel Sprays," SAE Paper No. 860469.

Saito, A., Kawamura, K., Watanabe, S., Takahashi, T., and Naoyuki, T., 1993, "Analysis of Impinging Spray Characteristics under High -Pressure Fuel Injection (1st Report, measurements of impinging spray characteristics)," *Trans, Jap. Soc. Mech. Engrs.* B, Vol. 59, pp. 3290～3295.

Sarre, C., Kong, S. and Reitz, R. D., 1999, "Modeling the Effects of Injector Nozzle Geometry on Diesel Sprays," SAE Paper No. 1999-01 -0912.

Senda, J., Yamada, K., Fujimoto, H., and Miki, H., 1988, "The Heat-Transfer Characteristics of a Small Droplet Impinging upon a Hot Surface," *JSME Int. Journal*, Series II, Vol. 31, No 1, pp. 105～111.

Senda, J., Kobayashi, M., Iwashita, S., and Fujimoto, H., 1994, "Modeling of Diesel Spray Impingement on Flat Wall," *Int. Symp.* COMODIA 94, pp. 411～416.

Stanton, D. W. and Ruthland, C. J., 1996, "Mathematical Modeling of Wall Films Formed by Impinging Sprays," SAE paper No 960628.

Werlberger, P. and Cartellieri, W. P., 1987, "Fuel Injection and Combustion Phenomena in High Speed DI Diesel Engine Observed by Means of Endoscopic High Speed Photography," SAE Paper No. 870097.

Yarin, A. L. and Weiss, D. A., 1995, "Impact of Drops on Solid Surfaces: Self-Similar Capillary Waves, and Splashing as a New Type of Kinematic Discontinuity," *J. Fluid Mech*, Vol. 283, pp. 141～173.